

# HIGH QUALITY EARLY TIME LIGHT CURVES OF GRB 060206: IMPLICATIONS FOR GAMMA RAY BURST ENVIRONMENTS AND ENERGETICS

A. MONFARDINI<sup>1</sup>, S. KOBAYASHI, C. GUIDORZI, D. CARTER, C. G. MUNDELL,  
 D. F. BERSIER, A. GOMBOC<sup>2</sup>, A. MELANDRI, C. J. MOTTRAM, R. J. SMITH, I. A. STEELE  
 Astrophysics Research Institute, Liverpool John Moores University, Twelve Quays House, Birkenhead, CH41 1LD, UK  
*Draft version March 3, 2018*

## ABSTRACT

The 2-m robotic Liverpool Telescope (*LT*) reacted promptly to the high-redshift ( $z = 4.048$ ) gamma-ray burst GRB 060206. The afterglow was identified automatically and multicolor  $r'i'z'$  imaging program was triggered without human intervention. Combining our data with those obtained from later follow-ups provides a well-sampled optical light-curve from 5 minutes to  $>2d$  after the gamma event. The light-curve is highly structured with at least three bumps evident in the first 75 minutes, including a major rebrightening ( $\Delta r' \approx -1.6$  at  $t \approx 3000s$ ), interpreted as late energy injection. At early time ( $t \approx 440s$ ), we find evidence for fast ( $\Delta t_{rest} < 4s \ll t$ ) variability, indicating ongoing internal-engine activity. We emphasise that a low redshift GRB ( $z < 1$ ) with similar intrinsic properties would have been interpreted completely differently due to undersampling of the light curve in the rest frame at early times; the light-curve behaviour of GRB 060206 should therefore not be considered peculiar. Finally, although the observed late-time steepening of the optical light curve resembles a jet break if taken in isolation, the lack of a corresponding change in the X-ray slope rules out a jet-break interpretation. Traditionally, GRB jet breaks have been inferred from optical data in the absence of simultaneous X-ray data. We suggest therefore that current estimates of the jet opening angle distribution might be biased by events like GRB 060206. Consequently, the GRB explosion energy distribution and event rates may have to be revised.

*Subject headings:* gamma rays: bursts - cosmology: observations

## 1. INTRODUCTION

The *Swift* satellite (Gehrels et al. 2004), launched in November 2004 and specifically designed to study Gamma Ray Bursts, is providing an overall rate of about 100 real-time gamma localizations per year. A considerable fraction ( $\approx 75\%$ ) are reobserved within minutes by the on-board X-ray (*XRT*) and UV-optical (*UVOT*) narrow field-of-view instruments, whilst an increasing number of ground-based robotic facilities are participating actively in the worldwide follow-up program by responding rapidly to satellite alerts. As a result, the number of GRBs with early-time light curves and spectroscopically determined redshift has increased dramatically over the last 18 months. Thus, in addition to important recent results such as the detection of short burst afterglows and the observation of the most distant ( $z > 6$ ) GRB observed to date (Haislip et al. 2005; Antonelli et al. 2005)), the following facts are emerging: *a*) a higher mean redshift ( $z \approx 3$ ) for Swift GRBs (Jakobsson et al. 2006) compared with those detected in the pre-Swift era ( $z \approx 1$  (Berger et al. 2005)); *b*) 990123-like (Akerlof et al. 1999) prompt flashes are on average weaker and less frequent than expected; *c*) a population of faint bursts (truly *dark* only in absence of an early, deep follow-up) providing useful constraints on existing optical suppression models (Roming et al. 2005; Oates et al. 2006); *d*) huge, rapidly rising and decaying flares observed in the X-ray light-curves, indicating prob-

able late-time activity of the inner engine (Burrows et al. 2005). The growing evidence for continued activity of the central engine, the detailed physics of which remains elusive, and the opportunity to probe the interaction of expanding shells with the circumburst/interstellar medium, particularly at high redshift, demand dedicated prompt followup observing programs. Large robotic telescopes such as the 2-m Liverpool Telescope are optimised for such followup and are proving effective (Guidorzi et al. 2005, 2006).

Early afterglow light curves exhibit a considerable variety and rebrightenings (hereafter called *bumps*) are becoming more frequently observed. GRB 021004 (Bersier et al. 2003; Matheson et al. 2003; Holland et al. 2003) remains one of the best studied events ( $z = 2.335$ ) and a number of different models have been invoked to explain its temporal behaviour: variable density profile (Lazzati et al. 2002), passage of the break frequency (Kobayashi & Zhang 2003), refreshed shocks (Nakar et al. 2003; Björnsson et al. 2004; de Ugarte Postigo et al. 2005), angular dependence of the energy profile on the jet structure (Nakar et al. 2003). Another interesting case is GRB 030329 ( $z = 0.17$ ), preferably modeled according to the refreshed shocks (late energy-injections) scenario (Huang et al. 2006). In this case, initially slower shells catch up with the external shock front, which, in the meantime, is decelerating due to the interaction with the surrounding medium. The early afterglow of GRB 050502a ( $z = 3.793$ ) exhibited a smooth decay, well-fitted by a power-law with index  $\alpha = 1.2$  ( $F_\nu \propto t^{-\alpha}$ ), followed by an achromatic bump emerging at  $t_{rest} \approx 600s$  that has been interpreted by Guidorzi et al. (2005) as due to density clumps in a

Electronic address: (am, sk, crg, dxc, cgm, dfb, ag, axm, cjm, rjs, ias)@astrophysics.liverpool.ac.uk

<sup>1</sup> Also: ITC-IRST and INFN, Trento, via Sommarive, 18 38050 Povo (TN), Italy.

<sup>2</sup> Present address: FMF, University in Ljubljana, Jadranska 19, 1000 Ljubljana, Slovenia.

uniform medium. More recently, an increasing number of events, in particular at high- $z$ , exhibit rebrightenings (Rykoff et al. 2006; Stanek et al. 2006). These observations support the hypothesis such behaviour might not be unusual. We report here multicolor robotic observations of GRB 060206 carried out by the Liverpool Telescope (*LT*) and revealing a structured behaviour of the early lightcurve. The 2-m aperture of the *LT*, the optimal observing conditions and a precise SDSS pre-burst field calibration (Cool et al. 2006) contributed to the remarkable quality of the dataset. Timely later photometry from *RAPTOR* (Wozniak et al. 2006) and *MDM* (Stanek et al. 2006) allowed us to compile an exceptionally information-rich light-curve catching the different phases of the early afterglow.

## 2. OBSERVATIONS AND ANALYSIS

On 2006 Feb 06, 04:46:53 UT<sup>3</sup> *Swift-BAT* detected GRB 060206 (trigger 180455) at Galactic Coordinates  $l=78.07\text{deg}$ ,  $b=78.28\text{deg}$ <sup>4</sup> (3 arc-min 90% containment radius). In the 15 – 350 keV band the prompt gamma profile is well described by a single quasi-gaussian peak with duration  $7s \pm 2s$ . *Swift-XRT* began observing 65s after the BAT trigger time and entered the South Atlantic Anomaly soon afterwards (Morris et al. 2006). *UVOT* started the on-target monitoring practically at the same time. As usual, a number of ground-based facilities were activated to follow-up the event. The redshift has been spectroscopically measured to be  $z = 4.048$  (Fynbo et al. 2006). Robotically triggered photometric observations with the Liverpool Telescope began at  $t = 309s$  after the GRB, at an airmass of 1.01. A sequence of  $2 \times 3 \times 10s$   $r'$  exposures, named *detection mode*, aims at finding potential afterglow candidates and automatically triggers the best suitable early follow-up observing program. Details of the procedure are reported elsewhere by Guidorzi et al. (2006). In the GRB 060206 case, a repeated sequence of  $r'i'z'$  120s exposures was initiated. The afterglow is detected with high S/N in all the single exposures. Calibration was facilitated and greatly improved by the availability of SDSS pre-burst photometry (Cool et al. 2006). We adopted 5 calibrated star-like PSF field objects to adjust the zero-point of the single images. The zero points were stable throughout the observation sequence, and consistent with nominal LT values<sup>5</sup>. Photometry was carried out independently using the Starlink/GAIA and DoPHOT programs. The datasets are in complete agreement with each other, and the results have been combined to further reduce the systematics. Magnitudes are converted into flux densities  $F_\nu$  (mJy) following Fukugita et al. (1996). Results are summarized in Table 1.

Figure 1 shows the complete lightcurve of GRB 060206. 100 *RAPTOR* (Wozniak et al. 2006) and 101 *MDM* (Stanek et al. 2006) photometric points have been included together with selected GCNs. The *RAPTOR* unfiltered values, calibrated with respect to USNOB1.0-

R2 magnitudes (Wozniak et al. 2006), have been flux-recalibrated with respect to the earlier *LT* data. This is equivalent of shifting the *RAPTOR* data by +0.3 magnitudes. This approach relies on a relatively stable colour. At a first glance this assumption might look uncertain since we are actually presenting evidence of a spectral evolution across the bump. However, by assuming a realistic  $\Delta(r' - i')_{bump} \approx 0.4$ , a rather small  $\Delta r'_{sys} \approx -0.07$  is estimated. This systematic correction has been added to the synthetic  $r'$  late photometry data. In any case this isn't in any way affecting our conclusions. The *MDM* data, as in Stanek et al. (2006), have been shifted by +0.22 magnitudes with respect to *RAPTOR* and accordingly converted into physical units. *XRT* data have been processed with the ftool 'xrtpipeline' to produce cleaned level II event files, applying default screening constraints. We select only events with grade 0 for both *PC* (Photon Counting) and *WT* (Windowed Timing) modes. For *PC* mode, we initially considered a 20 pixel-radius circle centred on the source. From the PSF profile, it was clear the data were partially affected by pile-up; following Vaughan et al. (2006), we corrected for this by excluding photons within a 5-pixel radius inner circle and then renormalised the resulting light curve for the fraction of the PSF profile considered. Background spectrum and light curve have been taken from four 50-pixel radius circles with no sources. No significant pile-up was found to affect WT data, following the procedure described in Romano et al. (2006). We adopted empirical ancillary files for the spectra created with the ftool 'xrtmkarf'. We used the latest spectral response matrices in the Calibration Database (CALDB 2.3).

### 2.1. $r'$ Lightcurve Fit

The analytical model adopted for the fit, up to the break at  $\sim 3 \times 10^4$  s, is:

$$F_\nu(t) = \sum_j F_j \cdot \sqrt[n]{\frac{2}{(t/t_j)^{-\alpha_{1j} \cdot n} + (t/t_j)^{-\alpha_{2j} \cdot n}}} \quad (1)$$

This is the sum of a number of smoothly connected broken power-laws (Beuermann et al. 1999).  $\alpha_1$  and  $\alpha_2$  depend on  $j$  and are the exponents at  $t \ll t_j$  and  $t \gg t_j$  and  $t_j$  the bump (break) time. When  $\alpha_1 < 0$  and  $\alpha_2 > 0$ , a bump is produced. A typical light-curve break, on the other hand, is obtained when  $\alpha_1, \alpha_2 > 0$  and  $\alpha_2 \neq \alpha_1$ . The constant  $n$  controls the smoothness of the transitions, but has a relatively small influence in this context (see Table 2).  $F_j$  is the individual flux contribution at the bump (break) time. In the case of GRB 060206 the  $j$  index runs from 0 to 5 (see Figure 1). The  $j = 0$  segment is, by definition, associated with  $t_j = 0$  and is therefore a simple power-law fitting the earliest *LT* photometric points. The  $j = 1$  segment accounts for the sharp, earliest bump occurring at  $t \approx 440s$  and the subsequent decay. The next segment describes three  $r'$  points lying at  $t \approx 2000s$ . However, this fit at 2000s is not unique as one may also fit the flattening of the curve around this time with  $\Delta\alpha \approx -0.8$ , beginning immediately after  $t = 1200s$ . Although this scenario may seem simpler than introducing a bump component via  $j = 2$ , assuming an achromatic flattening in the  $r'$  band curve for  $t = 1200s : 1900s$  (constrained by  $r'$  sampling)

<sup>3</sup>  $t=0$  throughout the paper.

<sup>4</sup> According to Schlegel et al. (1998)  $E(B - V) = 0.013$ . The estimated extinction, from Cardelli et al. (1989) curve, is  $A_{r'} = 0.036$ ,  $A_{i'} = 0.027$  and  $A_{z'} = 0.019$ .

<sup>5</sup> Confirmed also by the CMT in La Palma. Nightly averaged atmospheric extinction:  $r' = 0.076$ . [http://www.ast.cam.ac.uk/~dwe/SRF/camc\\_extinction.html](http://www.ast.cam.ac.uk/~dwe/SRF/camc_extinction.html)

would in turn imply a rebrightening in  $z'$  and  $i'$ . This confirms that a bump is required in this time interval. In our analytical model the bump time is arbitrarily fixed to  $t_2 = 1500s$ , and the shape fixed by the earliest case template. The only variable is the peak flux  $F_2$  that is in any case non significantly affected by  $t_2$ . In other words, a small rebrightening at  $t \approx 1500s$  is necessary because it is not possible to fit the light curve in all 3 colors ( $r'i'z'$ ) without including a bump at that time. The next segments,  $j = 3, 4$  provide a good fit to the biggest double-peaked bump ( $t_3 = 3529s \pm 26s$ ,  $t_4 = 5234s \pm 79s$ ). Most importantly, the cosmological time dilation ( $1+z$ ) implies that the intense activity described so far took place in less than 15 minutes in the rest frame. The last feature before the final break, possibly associated to a density variation, takes place at  $t \approx 16000s$  and is well described by the  $j = 5$  term. In absence of a systematic photometric sampling close to the late break ( $t \approx 0.6d$ ), we fitted the  $t > 1d$  MDM points with a simple, independent power-law. The analytical model validity is thus limited to  $t < 50000s$ , before the occurrence of the inferred break. The result is a steepening from  $\alpha_1 = 0.95$  ( $t < t_{break}$ ) to  $\alpha_2 \approx 1.8$  ( $t > t_{break}$ ). We note that these values differ slightly from those found by Stanek et al. (2006) who derived  $\alpha_1 \sim 0.7$  to  $\alpha_2 \approx 2.0$ . The difference is to be attributed probably to the  $j = 5$  bump that is recognized as a separate feature in our view, but included in the general pre-bump slope in Stanek et al. (2006). That late break nature is discussed in more detail in the next Section.

The analytical model fit was performed separately in three different time ranges:  $300 : 2500s$  (6 Degrees Of Freedom),  $2500s : 15000s$  (126 DOF) and  $7000s : 50000s$  (74 DOF). Since the fit parameters are common, the procedure is iterated to let them converge to the same values in the three intervals. Convergence is achieved after  $\sim 10$  iterations, and the result is then stable indicating that a true global minimum has been reached. A summary of the parameters resulting from the fit is reported in Table 2. In Figure 1 the single components are shown together with the resultant fitted curve.

## 2.2. Multi-epoch Spectral Energy Distribution Analysis

Figure 2 shows the pre-bump rest-frame SED interpolated at  $t = 785s$ , where the  $r'$  lightcurve is relatively smooth, from LT and XRT data. The XRT spectral shape at this epoch have been assumed coincident with the PC early template ( $t = 141s : 341s$ ). The X-ray flux at  $t = 785s$ , is derived from an  $\alpha = 1$  (Table 2) power-law extrapolation. This seems a quite reasonable assumption (see Figure 1). Further, no significant differences are seen between the XRT spectra extracted from PC and WT modes. An extrapolated UVOT-B point has been added to provide important qualitative constraints. The average time behaviour of the B light-curve is assumed to follow the well-sampled  $r'$  case. An  $F_{r'}(t)$  integral is performed over the UVOT time span ( $t = 1662s : 34946s$ , Boyd et al. (2006)). The averaged  $F_{r'}^{aver}$  is directly compared to  $F_B^{UVOT}$ . The following simple ratio relation provides an estimate of  $F_B$  corresponding to the pre-bump epoch of interest:

$$F_{r'}^{aver} : F_{r'}(T) = F_B^{UVOT} : F_B(T) \quad (2)$$

At  $t = 785s$  the four optical points are not reconcilable with a single power-law. The  $r'$  flux is slightly affected, according to Fynbo et al. (2006), by the deep Damped Lyman Alpha DLA absorption feature. The  $i'$  and  $z'$  values, on the other hand, can be very well extrapolated up to  $\nu_{rest} \approx 4840PHz$  following a rather typical  $\beta = 0.8$  slope ( $F_\nu \propto \nu^{-\beta}$ ). The UVOT-B point qualitatively confirms the pronounced HI absorption and is not included in the fitting procedure. Even if sparsely sampled, the positions of the  $i'$  and  $z'$  photometric points in the time interval  $t = 1000s : 3000s$  clearly indicate either a SED evolution or an additional unresolved activity (or both combined). A rigid shift<sup>6</sup> of the  $r'$  light-curve, interpreted either with the bump or the flattening, indicate that the  $i'$  and  $z'$  fluxes are significantly higher than expected. According to the photometric errors, the disagreement significance has been estimated in  $4\sigma$  in the bump scenario ( $i'$ ,  $9\sigma$  for  $z'$ ). Analogous results assuming an achromatic flattening ( $5\sigma$  and  $11\sigma$ ). We suggest that the SED evolution scenario is more conservative, but caution that a generally accepted quantitative picture would require better sampling of the light curves. As an additional note, we remark that the simple rescaling described in footnote is again able to account for the  $z'$  points calculated during the big bump rising slope. This might be a possible indication, even if not conclusive, that the SED is already relaxed before the bump reaches its peak.

In Figure 2 we show the post-bump SED at  $t = 5680s$  based on the PAIRITIEL JHK detections (Alatalo et al. 2006) ( $t_{start} = 2.91h$ ) and on the earliest MDM R point<sup>7</sup>. Both are back-extrapolated according to an  $\alpha = 0.95$  temporal slope (table 2). At this late time, already on the smooth side of the afterglow, the IR-X fluxes ( $\nu_{rest} = 0.7 : 8000PHz$ ) are well fitted by a common  $\beta = 0.93 \pm 0.02$  power-law ( $\chi^2/d.o.f. = 3.46/10$ ). However, a broken power-law with fixed indices  $\beta_{OPT} = 0.7$ ,  $\beta_X = 1.2$  is not ruled out ( $\chi^2/d.o.f. = 10.04/10$ ). The latter is considered in the light of the interpretative model discussed later.

Post-break IR photometry (Terada et al. 2006) and MDM late observations give  $\beta_{IR-O} = 0.7 \pm 0.3$ . A summary of the spectral results is given in Table 3.

## 3. DISCUSSION

### 3.1. Re-Brightening

After the remarkable rebrightening at  $\sim 1hr$  and before the break around  $t \sim 5 \times 10^4 s$ , the optical flux is described by a single power law with  $\alpha \sim 1$ , except small wiggles. This indicates that the blast wave radiating the afterglow had a significant transition from one Blandford-McKee (BM; Blandford&McKee 1976) solution to another BM solution around  $t = 1 hr$ . Since blast wave solutions depend only on two parameters (explosion energy and ambient density) possible scenarios are energy injection (Rees& Mészáros 1998; Kumar& Piran 2000; Sari & Mészáros 2000) and a density-jump medium

<sup>6</sup> The multiplicative factors for  $i'$  and  $z'$  are determined according to the earliest epoch and are respectively  $1.50 \pm 0.05$  and  $1.72 \pm 0.05$ .

<sup>7</sup> We adopted the original Stanek et al. (2006) R flux instead of the estimated  $r'$ . The SED is thus completely unaffected by the LT-to-RAPTOR conversion systematics described in detail in the text.

(Ramirez-Ruiz et al. 2001; Dai & Lu 2002). The degeneracy is broken by the X-ray observations. Since there is no signature of the cooling break in the decay phase of the X-ray afterglow (Morris et al. 2006), the X-ray band is likely to be located above the cooling frequency at  $t \sim 1$  hr. This implies a high ambient density, consistent with spectroscopic determinations (Fynbo et al. 2006). The late time break in the optical light curve also favors  $\nu_x > \nu_c$  at  $\sim 1$  hr as we will discuss below. If the X-ray band is above the cooling frequency, the flux does not depend on the ambient density (Freedman & Waxman 2001). We can conclude that the X-ray rebrightening is not due to a jump in the ambient density.

According to Kumar & Piran (2000), in the absence of a density enhancement, the flux depends on the explosion energy as:

$$F_\nu \propto E^{(p+3)/4} \quad \nu_m < \nu < \nu_c \quad (3)$$

$$F_\nu \propto E^{(p+2)/4} \quad \nu > \nu_c \quad (4)$$

Since the optical flux increased by a factor of  $\sim 4$ , the rebrightening indicates there was a huge impulsive energy injection  $\Delta E \sim 1.8E_0$  at  $\sim 1$  hr where  $E_0$  is the blast wave energy right before the rebrightening. A typical  $p=2.3$  value is assumed for the power-law distribution of electrons energies. Consistently with observations (Figure 1), the X-ray flux is expected to increase by a factor of 3. A rather smooth transition from one solution to the other at most wavelengths is expected. However, this is not the case at frequencies for which there is significant emission from the reverse shock (Kumar & Piran 2000; Kobayashi & Sari 2000). The sharp rise of the rebrightening implies that the typical frequency of the reverse shock is close to the optical band. The small wiggles before or after the major rebrightening can be explained by additional minor energy injection or density clumps in the ambient medium.

The energy injection is probably due to a decrease in the Lorentz factor of the outflow toward the end of the prompt GRB. This slow outflow collides with a blast wave when the blast wave have slowed down as a result of sweeping up the ambient material. Energy injection could also be caused by a long lasting activity of the central engine (Burrows et al. 2005). The energy in the blast wave at late times ( $> 1h$ ) is larger than that at the deceleration time by more than a factor of  $\sim 2.8$ . This requires the prompt gamma-ray emission process (internal shocks) to be more efficient than previously considered (Ioka et al. 2005; Nousek et al. 2006; Zhang et al. 2006; Granot, Königl & Piran 2006).

### 3.2. Jet Break?

The optical light curve of GRB 060206 steepened from  $\alpha = 0.95 \pm 0.02$  to  $1.79 \pm 0.11$  around  $t = (3 \sim 9) \times 10^4$  s. Although this steepening resembles a jet break, the X-ray light curve from  $t = 5 \times 10^3$  s to  $7 \times 10^5$  s remains consistent with a single unbroken power law decay with  $\alpha = 1.35 \pm 0.15$  (Morris et al. 2006). This clearly contradicts the monochromatic break predication by the jet model. In the wind model  $\rho(R) \propto R^{-s}$  (Chevalier & Li 1999), the cooling frequency  $\nu_c$  increases as a function of time  $\nu_c \propto t^{(3s-4)/(8-2s)}$ . The passage of the cooling frequency can produce a steepening of

$\delta\alpha = (3s - 4)/(16 - 4s)$  in the optical band first and in the X-ray later. The observed steepening  $\delta\alpha = 0.84$  gives  $s \sim 2.7$ . The cooling frequency rapidly increases as  $t^{1.7}$ , and it will cross the X-ray band around  $\sim 10^6$  s. The observed unbroken power law X-ray light curve up to  $t \sim 7 \times 10^5$  s is consistent. However, this scenario does not account for the difference of the decay indices between the pre-break optical ( $\alpha_{opt} = 0.95$ ) and the X-ray ( $\alpha_x = 1.35$ ) light curves, which should be on the same spectral segment and the decay rates should be identical to be consistent with the scenario.

A possible solution is that a blast wave initially propagates into a constant density medium  $\rho = m_p n$ , and around  $t \sim 3 \times 10^4$  s it breaks out in a wind-type  $\rho \propto R^{-s}$  medium. Using the isotropic gamma-ray energy about  $6 \times 10^{52}$  ergs (Palmer et al. 2006), the transition radius is estimated in equation (5) in which  $\zeta = (1 + z)/5$  and  $n_1 = n/10$  protons  $\text{cm}^{-3}$ :

$$R_{tr}(cm) \sim 3 \times 10^{17} \zeta^{-1/4} \left( \frac{t}{3 \times 10^4 s} \right)^{1/4} \left( \frac{E}{6 \times 10^{52} \text{ erg}} \right)^{1/4} n_1^{-1/4} \quad (5)$$

Although a large amount of energy is injected to the fireball after the prompt emission, the energy dependence of  $R_{tr}$  is rather weak. In this scenario, the order of the break and observational frequencies remains as  $\nu_m < \nu_{opt} < \nu_c < \nu_x$  after the major re-brightening  $t > 1$  hr. During the constant medium phase, the time and frequency dependences of the optical and X-ray flux are given by Equations (6) and (7) respectively (Sari, Piran & Narayan 1998):

$$F_{opt} \propto t^{-3(p-1)/4} \nu^{-(p-1)/2} \quad (6)$$

$$F_x \propto t^{-(3p-2)/4} \nu^{-p/2} \quad (7)$$

With the standard value of  $p = 2.3$  these give reasonable fits to the observational decay indices, while the estimated optical spectral index  $\beta \sim 0.7$  is slightly shallower than the observations  $\beta \sim 0.93 \pm 0.02$ . Moreover, a spectral break is not directly inferred between optical and X-ray that seem to lie on a single slope. However, as explained in the previous Section, the predicted  $\beta \sim 0.7$  value is not significantly ruled out when a broken power-law is invoked. When the blast wave propagates into a wind medium, as the ambient density decreases, the optical flux drops as  $F_{opt} \propto t^{-\alpha_w}$  where

$$\alpha_w = \frac{[2s + 3(p-1)(4-s)]}{(16-4s)} \sim 1.8 \quad (8)$$

for  $p=2.3$  and  $s=2.5$ . Since the X-ray band is above the cooling frequency, its flux does not depend on the ambient density, and the X-ray decay index does not change before and after the break-out. Considering the scaling between the observer time and blast wave radius  $t \propto R^{(4-s)}$ , the steep segment of the optical light curve requires that the ambient density should behave as  $R^{-2.5}$  between  $R_{tr}$  and  $\sim 3R_{tr}$ . The steepening from  $\alpha = 0.95$  to  $1.79$  in the optical light curve looks like a typical jet break. The X-ray light-curve, however, shows no sign of a change in decay slope. This conflicts with the jet break potential interpretation based on the optical light-curve. In most previous events, X-ray data are not available at

the “jet breaks”, and the breaks are interpreted based on optical data. The current estimate on the jet opening angle distribution might be biased by events like GRB 060206. Consequently, the GRB explosion energy distribution and the event rates may need to be reviewed.

#### 4. CONCLUSIONS

We presented a comprehensive study of the high redshift GRB 060206 based on early robotic observations, later published photometry, GCN circulars and Swift public data. The composite monochromatic light-curve is exceptionally well sampled and extremely structured. An early,  $\Delta t \ll t$  rebrightening suggests internal engine activity (internal shocks) continuing well beyond the gamma prompt emission. Later on, a high-significance *SED* evolution is inferred from multi-color  $r'i'z'$  photometry carried out by the Liverpool Telescope; this is probably associated with another pre-bump rebrightening. One hour after the GRB a significant, steep double-peaked rebrightening occurred, increasing the flux by a factor  $\sim 4$  with respect to the pre-bump values. We interpret the cause of this rebrightening to be due to a late-time energy injection. The energy in the blast wave at late time ( $t > 1h$ ) is a factor of 2.8 larger than that at the deceleration time, implying a higher internal shock efficiency than previously considered. Following the big bump, a rather typical spectral/temporal afterglow behaviour is observed, with a possible density variation fea-

ture superimposed on the smooth power-law decay. We interpret the fact that the steepening in the optical light-curve observed at  $t \approx 0.6d$  post-burst is not matched by similar behaviour in the X-ray as due to a transition in the density distribution of the ambient medium, likely from a constant density medium to a wind medium. In the absence of X-ray data the observed optical steepening would have been interpreted as a typical jet-break. Since most of the so far observed jet-breaks lack corresponding X-ray confirmation, we suggest that current estimate on the jet opening angle distribution might be biased by events like GRB 060206. The GRB explosion energy distribution and the event rates are thus potentially affected.

We thank P. O’Brien, J. Osborne, B. Zhang and D. Burrows for comments on the XRT observations and we are grateful to Prof. K.Z. Stanek for providing the MDM photometry table. CG and AG acknowledge their Marie Curie Fellowships from the European Commission. CGM acknowledges financial support from the Royal Society. AM acknowledges financial support from INFN and Provincia Autonoma di Trento. The Liverpool Telescope is operated on the island of La Palma by Liverpool John Moores University at the Observatorio del Roque de los Muchachos of the Instituto de Astrofísica de Canarias.

#### REFERENCES

- Akerlof, C., et al. 1999, *Nature*, 398, 400  
 Alatalo, K., et al. 2006, *GCN Circ.* 4702  
 Antonelli, L. A., Grazian, A., et al. 2005, *GCN Circ.* 3924  
 Aoki, K. et al. 2006, *GCN Circ.* 4703  
 Berger, E., et al. 2004, *ApJ*, 634, 501  
 Bersier, D., et al. 2003, *ApJ*, 584, L43  
 Beuermann, K., Hessmann, F.V. et al. 1999, *A&A*, 352, L26  
 Björnsson, G., Gudmundsson, E. H., & Jóhannesson, G. 2004, *ApJ*, 615, L77  
 Blandford, R.D. & McKee, C.F. 1976, *Phys. of Fluids*, 19, 1130  
 Boyd, P., et al. 2006, *GCN Circ.* 4722  
 Burrows, D. N. 2005, <http://arxiv.org/astro-ph/0511039>  
 Burrows, D. et al. 2005, *Science*, 309, 1833  
 Cardelli, J. A., Clayton, G. C., & Mathis, J. S. 1989, *ApJ*, 345, 245  
 Chevalier, R. A., & Li, Z.-Y. 1999, *ApJ*, 520, L29  
 Cool, R. J., 2006, *GCN Circ.* 4695  
 Dai, Z.G. & Lu, T. 2002, *ApJ*, 565, L87  
 de Ugarte Postigo, A. et al. 2005, *A&A*, in press, preprint (astro-ph/0506544)  
 Fukugita, M., et al. 1996, *AJ*, 111 Number 4, 1748  
 Freedman, D.L. & Waxman, E. 2001, *ApJ*, 547, 922  
 Fynbo, P. U., Dai, X. et al. 2006, astro-ph/0602444  
 Gehrels, N., et al. 2004, *ApJ*, 611, 1005  
 Granot, J., Königl, A. & Piran, T. 2006, submitted to *MNRAS*, astro-ph/0601056  
 Guidorzi, C., et al. 2005, *ApJ*, 630 Issue 2, L121  
 Guidorzi, C., et al. 2006, *PASP*, 118 N.840, 288  
 Haislip, J., et al. 2005, *GCN Circ.* 3915  
 Haislip, J., et al. 2006, *GCN Circ.* 4709  
 Holland, S., et al. 2003, *ApJ*, 582, L5  
 Huang, Y.F., Cheng, K.S., Gao, T.T. 2006, *ApJ*, 637, 873  
 Ioka, K., Toma, K., Yamazaki, R. & Nakamura, T. 2005, astro-ph/0511749  
 Jakobsson, P. et al. 2006, *A&A*, 447, 897  
 Kobayashi, S. & Sari, R. 2000, *ApJ*, 542, 819  
 Kobayashi, S. & Zhang, B. 2003 *ApJ*, 582, L75  
 Kumar, P. & Piran, T. 2000 *ApJ*, 532, 286  
 Lazzati, D., Rossi, E., Covino, S., Ghisellini, G., & Malesani, D. 2002, *A&A*, 396, L5  
 Malesani, D. et al. 2006, *GCN Circ.* 4706  
 Matheson, T., et al. 2003, *AJ*, 125, 2291  
 Morris, D. et al. 2006, *GCN Circ.* 4694  
 Morris, D. et al. 2006, *GCN Circ.* 4764  
 Nakar, E., Piran, T., Granot, J. 2003, *New Astronomy*, 8, 495  
 Nousek, J.A. et al. 2006, *ApJ*, in press, astro-ph/0508332  
 Oates, S., Mundell, C.G. et al. 2006, *MNRAS*, in preparation  
 Palmer, D. et al. 2006, *GCN Circ.* 4697  
 Ramirez-Ruiz, E., Dray, L.M., Madau, P. & Tout, C.A. 2001, *MNRAS*, 327, 829  
 Rees, M. & Mészáros, P. 1998, *ApJ*, 496, L1  
 Reichart, D. et al. 2006, *GCN Circ.* 4768  
 Roming, P. et al., 2005, astro-ph/0509273  
 Rykoff, E. S., Mangano, V. et al. 2006, *ApJ*, 638 Issue 1, L5  
 Romano, P. et al. 2006, *A&A*, submitted (astro-ph/0602497)  
 Sari, R. & Mészáros, P. 2000, *ApJ*, 535, L33  
 Sari, R., Piran, T. & Narayan, R. 1998, *ApJ*, 497, L17  
 Schlegel, D. J., Finkbeiner, D. P., & Davis, M. 1998, *ApJ*, 500, 525  
 Smith, J. A. et al. 2002, *AJ*, 123, 2121  
 Stanek, K. Z., Dai, X. et al. 2006, astro-ph/0602495  
 Terada, H., et al. 2006, *GCN Circ.* 4716  
 Vaughan, S. et al. 2006, *ApJ*, 638, 920  
 Wozniak, P. R., Vestrand, J.A., Wren, J.A., White, R.R., Evans, S.M., Caspersen, D. 2006, astro-ph/0602403  
 Zhang, B. et al. 2006, in preparation

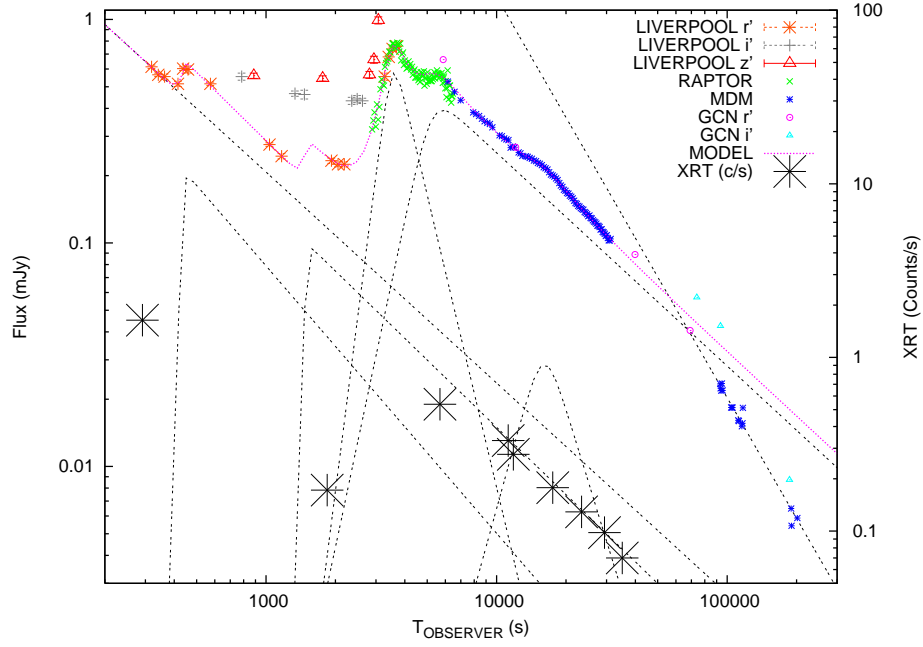


FIG. 1.— Complete GRB 060206 light-curve. Early ( $t < 3600s$ ) multi-color  $r'i'z'$  photometry from Liverpool Telescope robotic observations. Later data from Wozniak et al. (2006), Stanek et al. (2006), Malesani et al. (2006), Reichart et al. (2006), Haislip et al. (2006). Also shown: analytical model best fit, separate contributions (dotted lines), *XRT* counts rates (right-side axis).

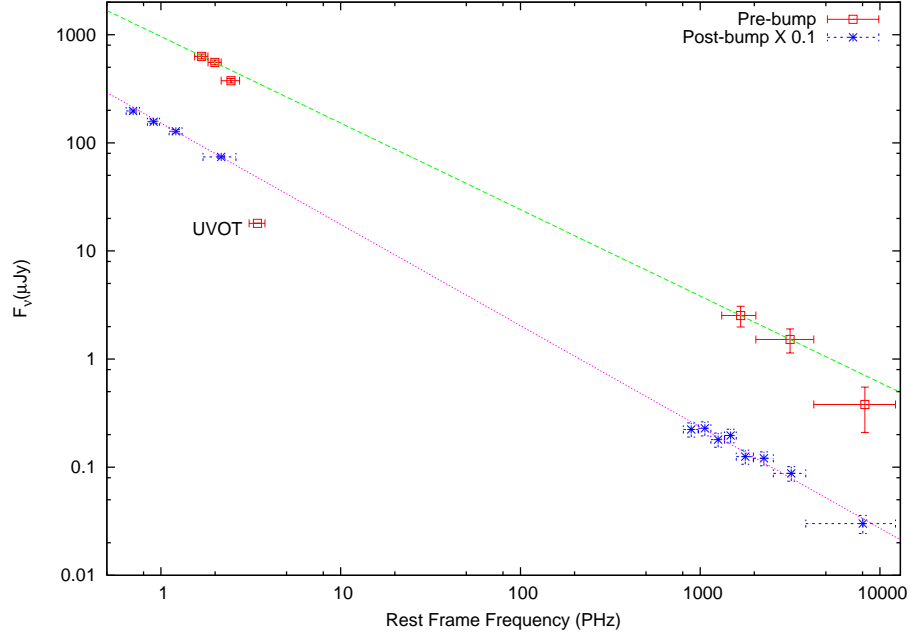


FIG. 2.— GRB 060206 pre- and post-bump Rest-frame SED ( $t = 785s$  and  $t = 5680s$ ). Optical points from Liverpool Telescope robotic observations, Stanek et al. (2006) and Boyd et al. (2006). The 5680s fluxes are divided by 10. Dotted lines:  $\beta = 0.80$  and  $\beta = 0.93$  power-law fitting respectively pre- and post-bump points. In the text we report evidence of a significant *SED* evolution occurring in  $t = 1000s : 3000s$ . The fit results are summarized in Table 3.

TABLE 1  
LIVERPOOL TELESCOPE GRB 060206 OPTICAL PHOTOMETRY

Filter	Epoch <sup>a</sup> (s)	Exposure (s)	Magnitude	Flux (mJy)
$r'$	319	10	$16.93 \pm 0.02$	$0.614 \pm 0.011$
$r'$	341	10	$17.02 \pm 0.02$	$0.565 \pm 0.010$
$r'$	363	10	$17.04 \pm 0.03$	$0.555 \pm 0.015$
$r'$	415	10	$17.12 \pm 0.03$	$0.515 \pm 0.014$
$r'$	437	10	$16.95 \pm 0.02$	$0.603 \pm 0.011$
$r'$	459	10	$16.96 \pm 0.04$	$0.597 \pm 0.021$
$r'$	574	30	$17.12 \pm 0.02$	$0.515 \pm 0.009$
$i'$	785	120	$17.04 \pm 0.04$	$0.555 \pm 0.020$
$z'$	885	120	$17.03 \pm 0.03$	$0.560 \pm 0.015$
$r'$	1036	120	$17.80 \pm 0.02$	$0.275 \pm 0.005$
$r'$	1169	120	$17.93 \pm 0.03$	$0.244 \pm 0.007$
$i'$	1336	120	$17.23 \pm 0.03$	$0.466 \pm 0.013$
$i'$	1487	120	$17.24 \pm 0.05$	$0.461 \pm 0.021$
$z'$	1762	120	$17.06 \pm 0.03$	$0.545 \pm 0.015$
$r'$	1921	120	$17.98 \pm 0.03$	$0.233 \pm 0.007$
$r'$	2052	120	$18.02 \pm 0.03$	$0.225 \pm 0.006$
$r'$	2185	120	$18.02 \pm 0.03$	$0.225 \pm 0.006$
$i'$	2355	120	$17.31 \pm 0.04$	$0.433 \pm 0.016$
$i'$	2487	120	$17.29 \pm 0.04$	$0.441 \pm 0.016$
$i'$	2619	120	$17.31 \pm 0.03$	$0.433 \pm 0.012$
$z'$	2807	120	$17.02 \pm 0.04$	$0.565 \pm 0.020$
$z'$	2939	120	$16.85 \pm 0.04$	$0.661 \pm 0.024$
$z'$	3071	120	$16.41 \pm 0.04$	$0.991 \pm 0.036$
$r'$	3273	120	$17.04 \pm 0.04$	$0.555 \pm 0.020$
$r'$	3405	120	$16.82 \pm 0.02$	$0.679 \pm 0.012$
$r'$	3538	120	$16.73 \pm 0.02$	$0.738 \pm 0.013$
$r'$	3670	120	$16.70 \pm 0.02$	$0.759 \pm 0.014$
.				

<sup>a</sup>Time delay with respect to the GRB trigger time,  $t_0 = 0.09302$  UT.

TABLE 2  
GRB 060206 SDSS-R LIGHTCURVE FIT RESULTS<sup>a,b,c</sup>

Segment	$F_j$ (mJy)	$\alpha_1$	$\alpha_2$	$t_j$ (s)	Comment
0	n.d.	n.d.	$0.94 \pm 0.17$	0	$\alpha_2$ =early slope
1	$0.160 \pm 0.016$	-30 (fixed)	$1.2 \pm 0.5$	$439 \pm 3$	
2	$0.076 \pm 0.007$	-30 (fixed)	1.0 (fixed)	1500 (fixed)	
3	$0.566 \pm 0.020$	$-8.0 \pm 0.5$	$4.3 \pm 0.6$	$3529 \pm 26$	big bump
4	$0.356 \pm 0.027$	$-4.9 \pm 0.7$	$0.95 \pm 0.02$	$5234 \pm 79$	$\alpha_2$ =post-bump slope
5	$0.029 \pm 0.002$	$-3.7 \pm 0.7$	$3.4 \pm 0.5$	$16037 \pm 397$	density bump
6	n.d.	n.d.	$1.79 \pm 0.11$	$\approx 53000$	$\alpha_2$ = slope after final break

<sup>a</sup>Refer to the text following equation 1 for an explanation.

<sup>b</sup>The  $n$  exponent is fixed to 2.5 for all the segments.

<sup>c</sup>The segment 6 has been fitted separately with a simple power-law.

TABLE 3  
FITTED SPECTRAL SLOPES FROM MULTI-EPOCH SED (FIGURE 2) AND TEXT

$Time(s)$	$\beta_O$	$\beta_X$	$\beta_{O-X}$	Comments
785	$1.42 \pm 0.58^a$	$1.15 \pm 0.55^b$	$0.81 \pm 0.03$	$\chi^2_{O-X}/d.o.f = 4.26/4$
$\approx 1800$	$2.05^c$	$1.15 \pm 0.55^b$	<i>n.d.</i>	$\beta_O \neq \beta_X$
5680	$0.84 \pm 0.14^d$	$0.84 \pm 0.15$	$0.93 \pm 0.02$	$\chi^2_{O-X}/d.o.f = 3.46/10$
$\approx 108000$	$0.7 \pm 0.3^e$	<i>n.c.</i>	<i>n.c.</i>	$\chi^2_{IR-O}/d.o.f = 0.85/1$

<sup>a</sup>Excluding B (UVOT) value affected by  $HI$  absorption

<sup>b</sup>Assumed from  $XRT$  spectrum in  $t = 141s - 341s$ . See text

<sup>c</sup>Calculated from  $r'i'z'$  points interpolated according the additional bump hypothesis (model-dependent)

<sup>d</sup>From back-extrapolations in  $JHK$  (PAIRITIEL) and  $R$  (MDM)

<sup>e</sup>SUBARU-IR & MDM-R